Heat Treat 2021: Proceedings of the 31st ASM Heat Treating Society Conference
September 14–16, 2021
America's Center, St. Louis, Missouri, USA
DOI: 10.31399/asm.cp.ht2021p0309

Modeling the Effect of Chemistry Changes on Phase Transformation Timing, Hardness, and Distortion in Carburized 8620 Gear Steel

Jason Meyer, Stefan Habean, Dan Londrico, Justin Sims
Dante Solutions, Inc., 7261 Engle Rd, Suite 105, Middleburg Heights, Ohio, 44130 United States
jason.meyer@dante-solutions.com
stefan.habean@dante-solutions.com
dan.londrico@dante-solutions.com
justin.sims@dante-solutions.com

Abstract

AISI 8620 low carbon steel is widely used due to its relatively low cost and excellent case hardening properties. The nominal chemistry of AISI 8620 can have a large range, affecting the phase transformation timing and final hardness of a carburized case. Different vendors and different heats of steel can have different chemistries under the same AISI 8620 range which will change the result of a well-established heat treatment process. Modeling the effects of alloy element variation can save countless hours and scrap costs while providing assurance that mechanical requirements are met. The DANTE model was validated using data from a previous publication and was used to study the effect of chemistry variations on hardness and phase transformation timing. Finally, a model of high and low chemistries was executed to observe the changes in hardness, retained austenite and residual stress caused by alloy variation within the validated heat treatment process.

Introduction

Carburizing low carbon steels to make them harder and more resistant to wear has been used since man began working with iron. From pack carburizing, to gas, vacuum, and even plasma carburizing, gas carburizing is the most widely used and easiest to maintain process control with modern equipment. Introducing higher concentrations of carbon to the surface of low carbon steel allows carbon to enter the part in a process called diffusion, creating a harder case while maintaining a softer core after quenching, due to the transformation of austenite to martensite in the carbon case. Compressive residual stress in the case allows the material to better handle bending stresses and surface wear present in applications utilizing gears and shafts. Therefore, carburization is a common practice in the automotive and aerospace industries. One of the most commonly carburized low carbon steels for gear applications is AISI 8620.

The above statement is an oversimplification, and the true carburization process has many variables that affect the results that need to be taken into account. These include, but are not limited to, temperature, time, carbon potential, steel chemistry, quench rate, and tempering temperature and duration. These variables affect the effective carbon case depth (ECD), and subsequent hardness, residual stress, and retained austenite profiles in the final carburized product. In this paper, a set of heat treatment schedules, differing only in time spent in the gas carburization process, were evaluated. The recipes were obtained from a study by Asi et al. [1], but for the purposes of this paper, only one recipe was chosen to investigate the variations in the chemical composition of the alloy.

Each heat of material produced can have a slight perturbation in alloy composition to the high and low tolerance limits of the specific steel grade. Thus, the ability to model the alloy composition of a particular material is sought. The goal of this paper is to model and simulate the experimental data from [1] using DANTE, and to further use this to investigate the effects of chemistry variations in the material on part behavior. Once validated, variations in alloy composition can be evaluated, including a 'low' chemistry and a 'high' chemistry. The investigation will show the effect on residual stress, hardness, and retained austenite caused by varying the chemical composition of AISI 8620.

Analysis

Methodology and Approach

Two recipes used for processing fatigue coupons were taken from [1], and were simulated using ANSYS, a commercial finite element analysis (FEA) package, with the DANTE material subroutines, used for heat treatment simulation. Here, ANSYS was coupled with DANTE's subroutines and material properties to handle the thermal-stress, and microstructural components of the simulation.

The CAD geometry of the fatigue coupon was constructed from the dimensions shown in Figure 1. However, only a one-tenth circumferential slice was modeled from the highlighted section in Figure 1. When constrained with proper, frictionless, boundary conditions, this model can allow for radial and axial growth and shrinkage on the internal edges. Reducing the computation cost of a full fatigue coupon model.

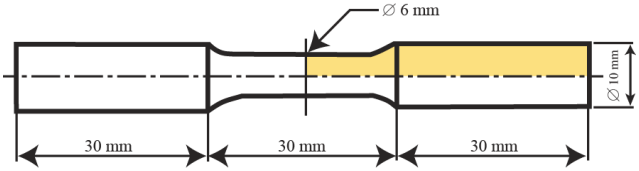

Figure 1: Fatigue coupon dimensions used in the analysis. The highlighted quadrant shows the slice used in the simulation

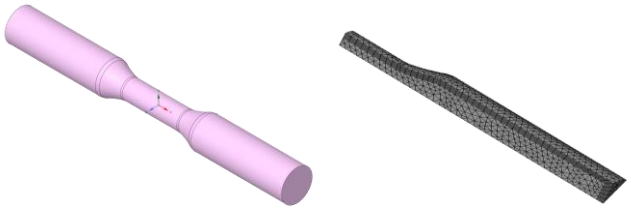

Figures 2 and 3: Figure 2 (left) shows the full CAD geometry of the fatigue coupon. Figure 3 (right) shows the meshed slice used in the simulation

Two gas carburization models were set up following the schedules in Table 1. The resultant carbon profiles were utilized in the DANTE thermal and stress models.

Table 1: Primary carburizing step time, temperature, and carbon potential for Group A and B recipes

Recipe	Time (min.)	Temp. (C)	Carb. Potential (%)
Group A	180	940	1.2
Group B	300	940	1.2

After initial carburization, the recipe included a step down in temperature and carbon potential to 850° C and 0.7 wt.% for 30 minutes followed by a direct oil quench, and a subsequent air cool to room temperature. The samples were then subjected to a one-hour temper at 170° C and finished with a final air cool to room temperature.

To further expand upon using computer simulation tools for predicting part and material performance from processing, an investigation into the effects of alloy variation from heat to heat of coupon material was executed. Here, recipe B from the two recipes used in the initial investigations was selected and simulated again, but this time using the material chemistry for an alloy lean ('low') heat and for an alloy rich ('high') heat of the 8620 material, with both chemistries being obtained from Rothman's work [2] and shown in Table 2, and the "nominal" composition being obtained from [1].

Alloy composition generally varies from heat to heat, with even the slightest change in a constituent element affecting the overall hardenability of the steel. For example, chromium has a significant effect on hardenability and corrosion resistance, however large amounts can cause the steel to become too hard and prone to cracking. Molybdenum is a strong carbide former and most notably increases high temperature strength. Nickel helps retain some ductility and toughness after hardening as well as increasing low temperature strength. Silicon has an important role in deoxidation of the steel, while phosphorus and sulfur are considered impurities and they typically have upper limits as to the amount allowable in each steel grade. Manganese also aids in deoxidation while preventing iron sulfides and inclusions in the steel. Carbon is arguably the most important alloy when it comes to hardenability, hardness, and tensile strength, and is the main reason low carbon steels are carburized.

Table 2: Compositions used for nominal, low, and high alloy simulations. Note that the nominal chemistry is from [1]

	Nominal (wt%)	Low (wt%)	High (wt%)
C	0.197	0.18	0.23
Mn	0.71	0.70	0.90
P	0.00	0.00	0.035
S	0.01	0.00	0.04
Si	0.21	0.15	0.30
Ni	0.45	0.40	0.70
Cr	0.41	0.40	0.60
Mo	0.15	0.15	0.25

These hardenability changes can be best demonstrated through continuous cooling (CCT) and isothermal (TTT) phase diagrams. In this case, Figure 4 shows the ferrite-pearlite and bainite isothermal transformation lines for the uncarburized nominal composition for 8620 generated by a TTT generator utility from DANTE Solutions. Figure 5 shows the same information but for the high alloy and carbon composition for the material. Note that due to the low and nominal compositions being nearly identical, the TTT plots were as well, and as such the low alloy plot is not included. As can be seen between the nominal and high alloy plots, the hardenability shifts noticeably to the right, even with the relatively small alloy changes. These differences will inevitably lead to differences in the heat treatment response of the material, leading to changes in final mechanical properties.

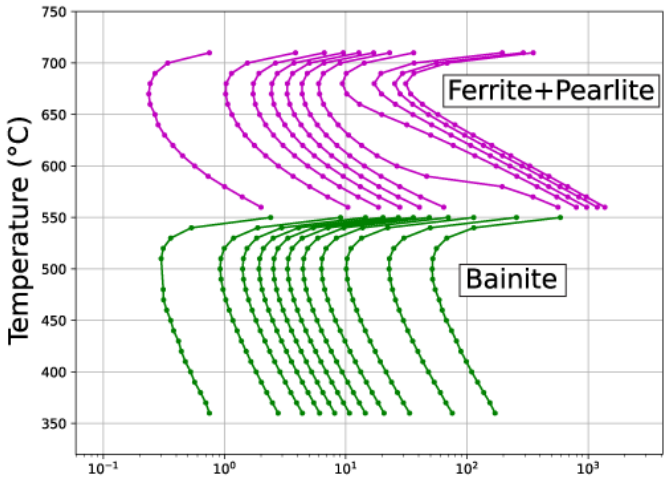

Figure 4: TTT plot demonstrating the ferrite and pearlite (purple) and bainite transformation (green) timings for nominal composition 8620

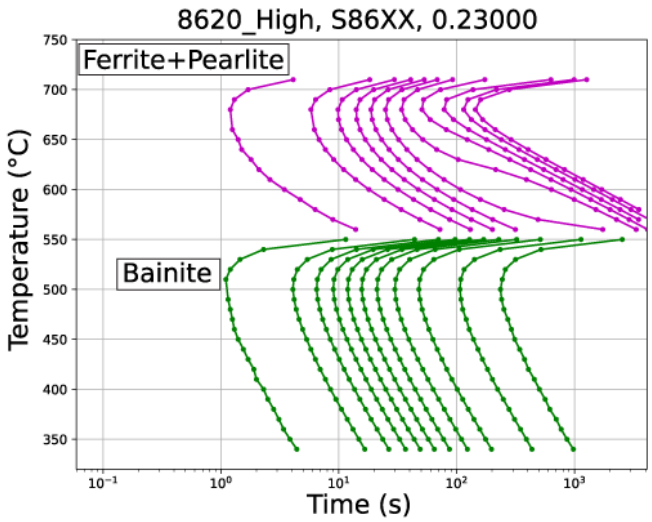

Figure 5: TTT plot demonstrating the ferrite and pearlite (purple) and bainite transformation (green) timings for high alloy composition 8620

These high and low alloy ranges were investigated using the same methodology listed previously, and the results of this investigation were then compared with those of the nominal composition used prior, to demonstrate how even slight changes in chemistry of a material can impact its hardenability, and thus its response to heat treatment. An adequate heat treatment simulation model should have the capability to account for slight variations in chemistry ranges. The DANTE software has such capabilities.

Results

Model Validation

To validate the DANTE model, the simulation results for the nominal chemistry were compared to the experimental results presented by Asi et al. [1]. The authors report values on residual stress, hardness, and retained austenite. The authors in [1] report using Vickers hardness scale for hardness measurements and X-ray diffraction for retained austenite and residual stress measurements. Simulated carbon profiles are also reported here, as the carbon distribution is critical to the final part properties and mechanical performance. Measured depth profiles were extracted from the path shown in Figure 6.

For the two heat treatment recipes (Groups A and B), measured residual stress was compared to simulation results shown in Figure 7. While the results were similar between the two processes, Group A shows slightly higher compression until about 0.4 mm where Group B becomes more compressive, agreeing reasonably with the experimental results. The high spike in compressive stress on the near surface for the experimental data is typically indicative of a deformation during the quench or surface finishing after the process. This profile can be caused by an extremely high quench rate at the near surface of the sample. Unfortunately, the generalized oil quench rate that was applied to this process could not capture this effect. Regardless, the overall trend of the simulation beyond this zone agrees reasonably with the experimental results.

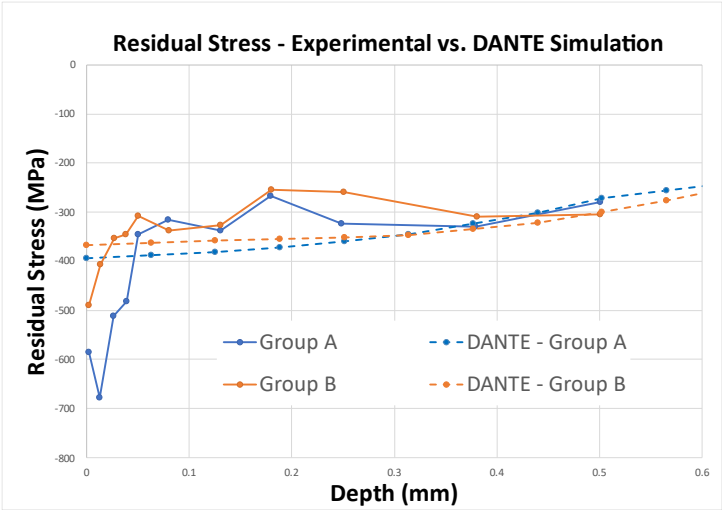

Figure 7: Experimental and simulation residual stress results

Hardness comparisons are shown in Figure 8. The Group B match is excellent, with the Group A matching well at the case depth but slightly lower than the experimental results at the surface. Here, the two vertical bars on the plot represent the respective effective case depth (ECD) for each group, defined as 550 HV. It is important to note that the Group B case is significantly deeper than that of Group A. This is due to the increased carburization time of 300 minutes (for Group B) from 180 minutes (Group A). This extra two hours of carburization time allows the carbon to diffuse further into the coupon, producing a deeper case.

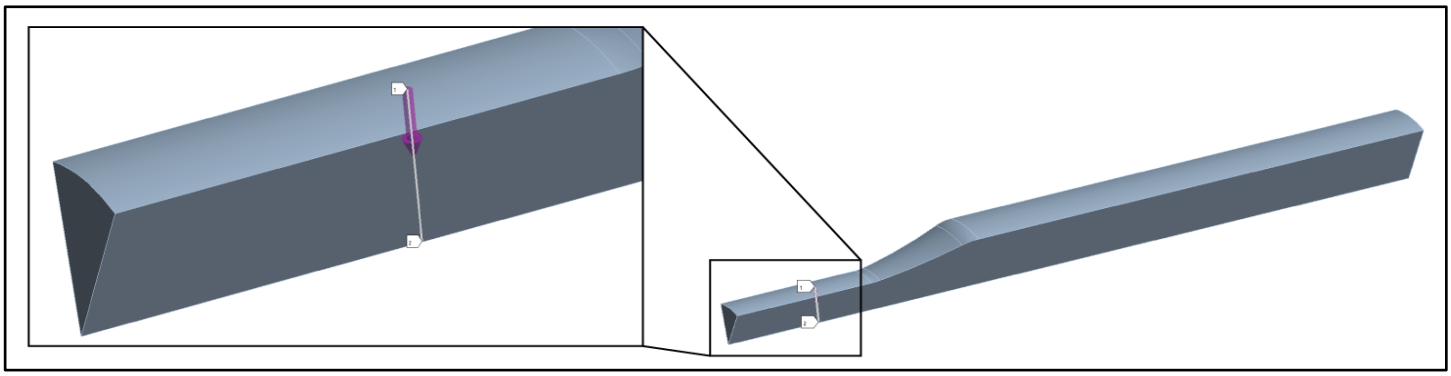

Figure 6: Simulated data was obtained from a path profile

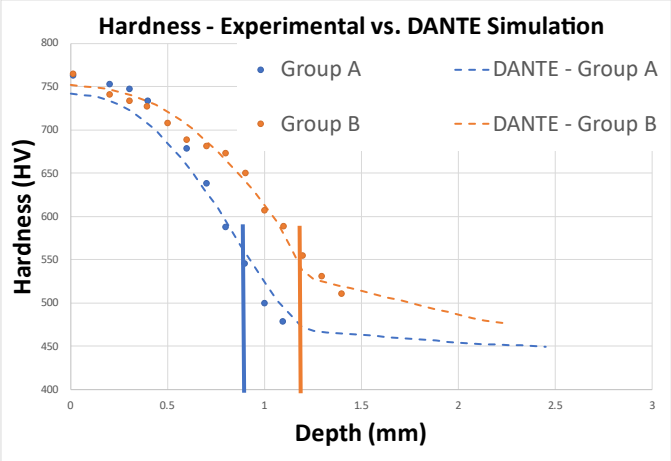

Figure 8: Experimental and simulation hardness results, with the vertical lines representing the approximate ECD for Group A(blue) and B (orange)

The retained austenite values between groups A and B agree reasonably with the data from [1] as shown in Figure 9. The trend of group A follows the downward trend into the core and the difference is about 1%.

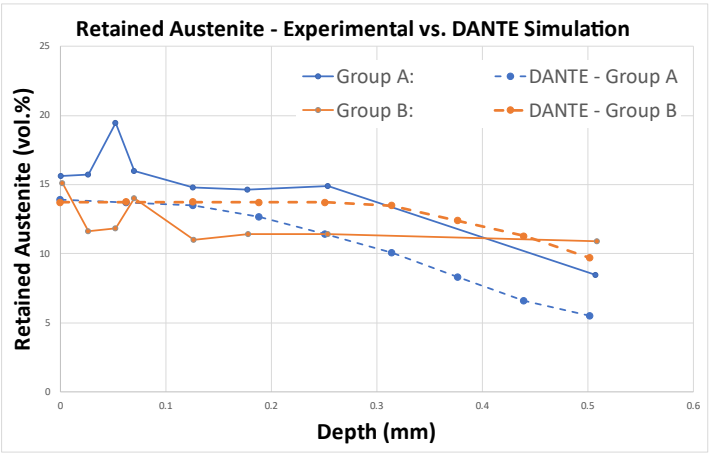

Figure 9: Experimental and simulation retained austenite results

The DANTE simulation results match quite well with the experimental data, especially the hardness values.

Simulated Carbon Case Profiles

For the Group A and Group B gas carburization recipes, the simulated case-core carbon profiles are plotted as a function of surface depth. Figure 10 shows the carbon case profile for the Group A schedule, and the vertical line shown gives the approximate location of the effective case depth.

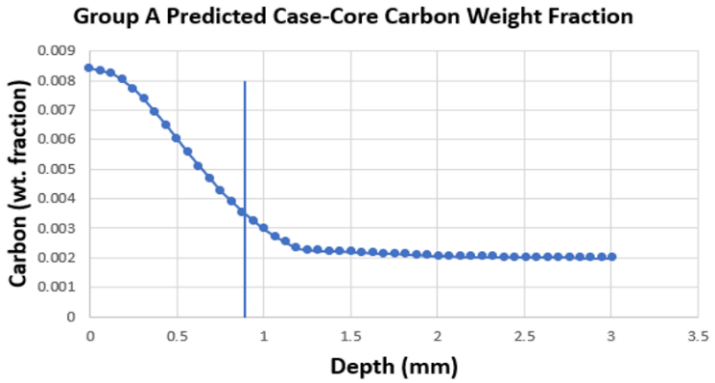

Figure 10: Group A model carbon case, with the vertical blue line representing the approximate ECD

Figure 11 shows the carbon case profile for the Group B schedule, and the vertical line shown gives the approximate location of the effective case depth. Beyond the case, the carbon quickly drops down to the material's base carbon for Group A, while Group B shows a more gradual decrease from case to core ending up just above 0.197 wt% base carbon.

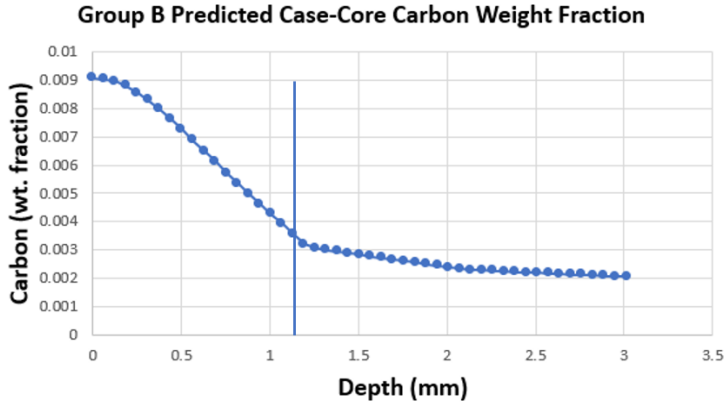

Figure 11: Group B model carbon case, with the vertical blue line representing the approximate ECD

The effective case depth was reported from [1] for Group A and B to be when the hardness reaches 550 HV and a depth of 0.86 mm and 1.2 mm, respectively, again shown in Figure 8 were reported. For the DANTE simulation, the ECD for Groups A and B were found to be 0.9 mm and 1.16 mm, respectively. The predicted values agree well with the experimental results. With the validated model, modifications can now be made to the chemistry ranges of the model.

Low and High Chemistry Models: Simulated Results

To evaluate the effects of alloy composition variation, Group B was chosen, and models were executed with high and low chemistry ranges. These were further explored through the residual stress (Figure 12), hardness (Figure 13), and retained austenite profiles (Figure 14), as well as with a comparison of the end length distortion (elongation) of the components (Table 3).

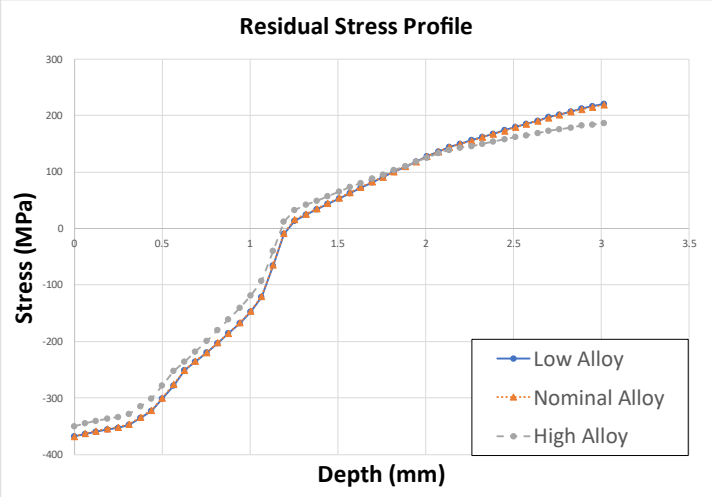

Figure 12: Simulated low, nominal, and high chemistry range residual stress

The hardness profiles for the low, nominal, and high compositions are nearly identical in the case, and start to differ amongst compositions in the core section. This is shown in Figure 13 and corresponds to the Martensite distribution after quench, shown later in Figure 15.

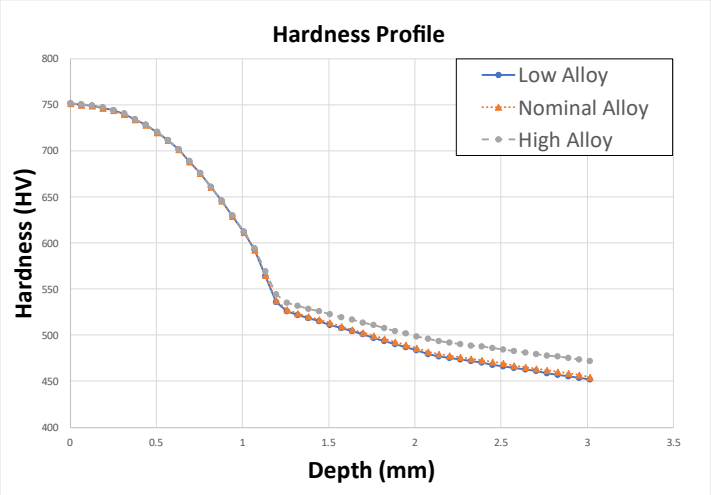

Figure 13: Simulated low, nominal, and high chemistry range hardness results

The retained Austenite profiles shown in Figure 14 are nearly identical in the case section of the model, and the higher case residual Austenite is due to the carbon profile after carburization. The differences seen in the core section correspond to the differences in hardenability amongst the three chemistries. The high alloy composition produces more core Martensite after processing, allowing for more retained Austenite in this section. Whereas the low and nominal chemistries produce less core Martensite and more diffusive phases, consuming the Austenite in the core.

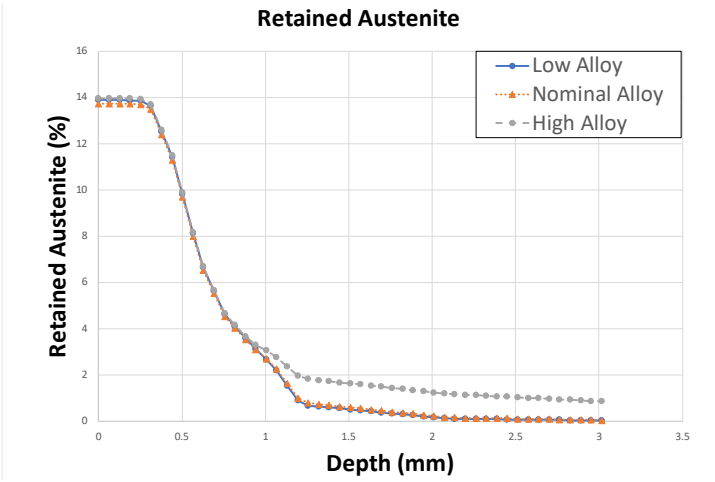

Figure 14: Simulated low, nominal, and high chemistry range retained austenite

Although not reported in [1], length distortion of the Group B sample along its axial direction for the low, nominal, and high chemistry ranges are also reported here. In general, as the amount of alloy increased, so did the axial distortion of the sample. It is important to note that the axial length distortion presented here is for the simulated half model. The total length change is actually twice the values shown in the table due to the symmetry boundary condition.

Table 3: Simulated low, nominal, and high chemistry axial length distortion along the centerline of the sample

Model Chemistry	Length Distortion (mm)
Low	0.011848
Nominal	0.014305
High	0.034790

Discussion

Comparison of Simulation Results to Experimental Data

Overall, the simulation results are in good agreement with the experimental data, with the simulations accurately capturing the hardness profile, and capturing the trends for the residual stress and austenite data. It is important to note that the x-ray diffraction and metallographic techniques used to experimentally determine residual stress and retained austenite generally have some point-to-point error which may be the cause of the unevenness in Figures 7 and 9.

However, despite this, the simulation results are still able to capture the overall trends and are in good agreement with the measured values of these data sets. Additionally, the carbon profile was never given in [1], but because of how well the hardness and retained austenite simulation results match the experimental data, we assert that the simulation accurately captured the carbon profiles of the physical components.

The discrepancies at the surface in the residual stress states can be attributed to plastic deformation in the region. This may have been brought about due to an incredibly intensive quench or work hardening after the process.

Chemistry Variation

The hardenability differences demonstrated through the TTT plots in Figures 4 and 5 did in fact manifest in the simulations. This can be seen especially in the hardness and residual stress plots. In these, the sub case hardness and retained austenite is noticeably higher in the high alloy part. This is primarily due to the increase in hardenability and in the material base carbon leading to an increase in sub case martensite. The difference in sub case martensite becomes rather significant as well, topping out at a 13% difference in martensite at the core of the part with the high alloy chemistry compared to the low and nominal profiles as shown in Figure 15 below.

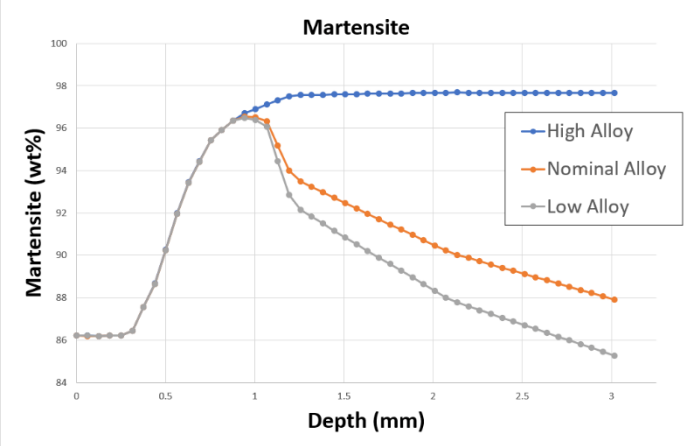

Figure 15: Simulated low, nominal, and high chemistry range Martensite profiles

Since carbon plays the most significant role on hardenability, it can be attributed to the consistency between the low, nominal, and high results in the case. However, some deviation begins to occur in the sub-case, where the effects of varying the alloy composition becomes more pronounced. Nevertheless, the composition differences are larger between the nominal and high chemistries than the low and nominal chemistries. This can also explain why the nominal and low chemistry results are more like each other.

When modeling steel grades, the ability to modify the hardenability by providing the specific chemical composition is another benefit of a good heat treatment simulation model.

Future Considerations

Computer simulation can be a powerful tool for predicting material and part behavior during processing. While the models used have been well explored and validated, there is still space for the development of new models for material processing. One challenge is the development of new material properties for carburizing temperatures and potentials at non-typical or non-traditional gas carburization conditions. Modeling carbon diffusion requires diffusivity data for a whole spectrum of range of carbon potentials used. In this study, the diffusivity data was obtained via the DANTE material database. More data may be obtained experimentally in the future for a specific material and condition set and added to the database for simulations.

Another future consideration is that in [1], it is noted that intergranular oxides were observed in the surface of the parts, due to unprotected processing at high temperatures. The processing conditions affect the boundary conditions used to model these effective phenomena. So in a practical setting, a more adequate characterization of the equipment can prove effective.

Conclusion

In conclusion, a brief investigation into the effects of heat treating 8620 material was conducted using DANTE, a commercially available heat treatment FEA simulation software package. Experimental and simulation data fit well and were used to further investigate the effects of a low and high chemistry for the steel. Practically, the significance of a heat treatment model to account for slight variations in chemistry allows the user to enter in the exact specifications of a part material, thus increasing the fidelity of the model. While changes in alloy chemistry do not appear significant for 8620, larger alloy variations make a difference.

References

[1] O. Asi, et al., “The effect of high temperature gas carburizing on bending fatigue strength of SAE 8620 steel,” Elsevier, Materials and Design, 30, (2009), July, 22, 2008

[2] Rothman, M.F., “High-Temperature Property Data: Ferrous Alloys”, ASM International, Metals Park,OH (1989)

[3] Chandler, H., *Heat Treater’s Guide, Second Edition*, ASM International, Metals Park, OH (1995)